Journal of Theoretical Biology 547 (2022) 111150

Contents lists available at ScienceDirect

Journal of Theoretical Biology

journal homepage: www.elsevier.com/locate/yjtbi

# Hormonal regulation of ovarian follicle growth in humans: Model-based exploration of cycle variability and parameter sensitivities

Sophie Fischer-Holzhausen *, Susanna Röblitz

*Computational Biology Unit, Department of Informatics, University of Bergen, Bergen, Norway*

ARTICLE INFO

*Article history:*
Received 17 December 2021
Revised 23 March 2022
Accepted 28 April 2022
Available online 11 May 2022

*Keywords:*
HPG axis
Reproductive hormones
Mathematical modelling
Stochastic dynamical system

ABSTRACT

We present a modelling and simulation framework for the dynamics of ovarian follicles and key hormones along the hypothalamic-pituitary–gonadal axis throughout consecutive human menstrual cycles. All simulation results (hormone concentrations and ovarian follicle sizes) are in biological units and can easily be compared to clinical data. The model takes into account variability in follicles' response to stimulating hormones, which introduces variability between cycles. The growth of ovarian follicles in waves is an emergent property in our model simulations and further supports the hypothesis that follicular waves are also present in humans. We use Approximate Bayesian Computation and cluster analysis to construct a population of virtual subjects and to study parameter distributions and sensitivities. The model can be used to compare and optimize treatment protocols for ovarian hyperstimulation, thus potentially forming the integral part of a clinical decision support system in reproductive endocrinology.



## 1. Introduction

The interplay between the hypothalamus, the pituitary gland and the gonadal glands regulates and maintains the menstrual cycle. Gonadotropin-releasing hormone (GnRH) is responsible for the release of the two gonadotropins: follicle stimulating hormone (FSH) and luteinizing hormone (LH) from the pituitary gland. Gonadotropins have feedback actions on folliculogenesis, meaning the maturation of the ovarian follicle, and thereby the production of ovarian hormones. In turn, ovarian hormones such as estradiol (E2) and progesterone (P4) affect LH and FSH release both directly and indirectly via GnRH signalling (Speroff and Fritz, 2005).

In this work, we present a nonlinear differential–algebraic system of equations (DAEs) to model the time-evolution of these five key hormones and the growth dynamics of ovarian follicles. The mechanistic model adopts the interplay of these five hormones from previously published models of the menstrual cycle (Clark et al., 2003; Reinecke and Deuflhard, 2007; Röblitz et al., 2013). As a novelty, our model connects the hormone dynamics to the time evolution of the diameter of ovarian follicles. Since the unit of the follicular diameter is given in units of millimeter, our simulation results can be compared to ultrasound measurements. Every emerging follicle is described by an ordinary differential equation (ODE) with follicle specific parameters. The work of Lange et al. (2019) inspired the mathematical formulation of the follicular growth. The coupling of the follicle model to a hormone dynamics model makes it possible to perform in silico studies of the interplay between sex hormones and follicular growth behaviour during normal menstrual cycles, as well as under ovarian hyperstimulation treatment conditions (Fischer et al., 2021).

In a series of articles Schlosser, Selgrade, and Harris-Clark introduced a mathematical model of the hormone control system (Selgrade, 2001; Clark et al., 2003). Their model combines pituitary hormone dynamics of LH and FSH with the dynamics of the ovarian hormones P4, E2, and inhibin. Reinecke and Deuflhard (2007) expanded and modified the model from Clark et al. (2003). Major changes were the incorporation of a GnRH pulse generator responsible for the release of GnRH, equations for the GnRH concentration, receptor binding mechanisms and addition of further feedback interactions to LH, FSH, and ovarian hormone dynamics. Röblitz et al. (2013) added further mechanistic details and re-parameterized the model from Reinecke and Deuflhard (2007) in order to simulate treatments with GnRH analogues. Mathematical models and numerical simulations have proven themselves useful to get a better understanding of various aspects of the menstrual cycle, for example to study the polycystic ovary syndrome (PCOS) (Chavez-Ross et al., 1997), to create virtual patient cohorts for in silico clinical trials (Sinisi et al., 2020; Sinisi et al., 2020), or to simulate ovarian stimulation protocols (Reinecke and Deuflhard, 2007; Fischer et al., 2021).

* Corresponding author at: Institute of Informatics, University of Bergen, Bergen, Norway.
*E-mail address:* sophie.fischer@uib.no (S. Fischer-Holzhausen).

https://doi.org/10.1016/j.jtbi.2022.111150
0022-5193/

Ovarian hormone dynamics and the growth behaviour of ovarian follicles are closely associated. Their interactions are crucial to enable female fertility. The literature contains different approaches for modelling follicle growth. The work by Selgrade (2001) and Clark et al. (2003) used the description of follicular masses in discrete stages to simulate folliculogenesis. As a result, the discrete number of active follicles is unknown in the model. Another approach focused on the cellular activity of theca and granulosa cells (Clément et al., 1997). Both cell types play an essential role in ovarian hormone production. The authors in Reinecke and Deuflhard (2007) proposed combining the first two approaches by describing a granulosa- and a theca-cell mass instead of a follicluar mass, thereby focusing on the location of ovarian hormone production. An entirely different approach is modeling the dynamics of single follicles instead of follicular or cellular masses (Lacker and Akin, 1988; Chavez-Ross et al., 1997; Lange et al., 2019). The simulation of individual follicles allows for the comparison to ultrasound measurements (Lange et al., 2019) and for observing pathological behaviour such as PCOS (Chavez-Ross et al., 1997).

In this paper, we combine the approaches from Röblitz et al. (2013) and Lange et al. (2019) into a model that couples hormone dynamics with the growth dynamics of individual follicles. Compared to already existing approaches, our model is the first model that can be used to simulate both hormone concentrations and follicle sizes throughout consecutive menstrual cycles, with or without ovarian stimulation treatment. The two key questions we want to answer with our model are the following. Does follicular competition combined with hormone dynamics result in follicular waves? Are there single parameters that are particularly sensitive for cycle length, follicular count, or abnormal hormone profiles? In this paper, we address these two questions by running simulations and by combining a search in parameter space with model-checking techniques for parameter space exploration. The model is evaluated quantitatively by using hormone profile data. Its predictive power has been tested previously in Fischer et al. (2021), where we showcased the use of the coupled model to perform a simulation based study of ovarian hyper-stimulation protocols. In the following, we introduce this modelling and simulation framework for the menstrual cycle in more detail.

## 2. Model construction and biological background

The flowchart in Fig. 1 gives an abstract representation of the interaction network governing the menstrual cycle. The hypothalamus releases GnRH in a pulse fashion. GnRH stimulates the synthesis and release of pituitary hormones LH and FSH (Marshall and Griffin, 1993). In the ovaries, LH and FSH regulate folliculogenesis. Each growing follicle faces one of two fates: either apoptosis or becoming the dominant follicle, which releases its egg cell during ovulation. The remaining parts of the dominant follicle transform into the corpus luteum. Follicles are recruited in cohorts and the majority of recruited follicles undergo apoptosis (Fortune, 1994). Growing follicles are the main source of E2, while the corpus luteum produces both E2 and P4. Through the blood stream, E2 and P4 arrive at the hypothalamus and the pituitary gland, where their feedback interactions modulate the GnRH, LH and FSH dynamics. This process results in quasi-periodic hormone profiles with a cycle length of 25 to 35 days (Bakos et al., 1994; Harlow, 2000; Bull et al., 2019). However, the average cycle length shows a high variability between women and is age-dependent. One cycle consists of two characteristic phases: the follicular phase and the luteal phase. The ovulation of one follicle, in rare events also multiple follicles, separates the two phases. The timing of ovulation mainly determines the cycle length. Therefore, the observed fluctuations in the length of the follicular phase are larger than those in the luteal phase (Bull et al., 2019).

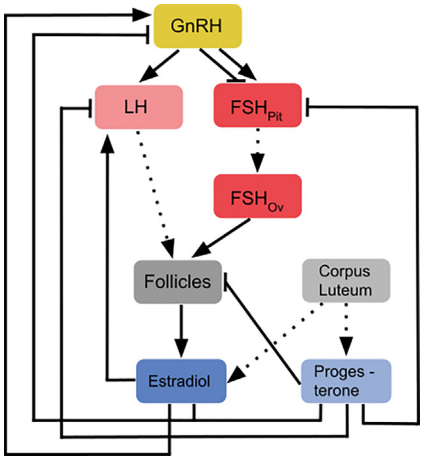


**Fig. 1.** Flowchart of key mechanisms of the menstrual cycle. Solid lines indicated feedback interactions encoded in the model. Positive feedback is encoded by arrows and negative feedback is presented by bars. Dotted lines represent the following other types of interactions: FSH release from the pituitary to the blood, the LH concentration dependent ovulation of dominant follicles, and the production of E2 and P4 by the corpus luteum. Reading the figure from top to bottom, the endocrine signalling that runs the menstrual cycle can be summed up as follows. GnRH stimulates LH. FSH is both stimulated and inhibited by GnRH. LH and FSH effect follicular maturation. Growing follicles produce E2, which stimulates the release of LH. A sufficiently high LH concentration triggers the ovulation of a follicle which then transitions into the corpus luteum. The simultaneous release of E2 and P4 by the corpus luteum inhibits the release of GnRH. Additionally, P4 has an inhibitory effect on LH and FSH. E2 stimulates or inhibits GnRH concentration dependent on the E2 concentration.

Our model is formulated as a semi-explicit differential–algebraic system of the form:

$$\begin{aligned} \tfrac{dx}{dt} &= f(t, x(t,\theta), y(t,\theta)) \\ 0 &= g(t, x(t,\theta), y(t,\theta)), \end{aligned} \tag{1}$$

with a pair of state variables $(x(t,\theta), y(t,\theta))$ depending on the time $t$ and parameters $\theta$. The dynamics of $x(t,\theta)$ are described by ODEs, whereas the dynamics of $y(t,\theta)$ are described by algebraic equations.

Since feedback interactions are often unknown or too complex to be modeled in detail, Hill functions are a common tool to describe feedback interactions in a qualitative manner. Stimulatory functions ($H^+$) and inhibitory functions ($H^-$) are given by the following equations:

$$\begin{aligned} H^+\left(S_i, T_i^j, n_i^j\right) &= \frac{\left(S_i/T_i^j\right)^{n_i^j}}{1+\left(S_i/T_i^j\right)^{n_i^j}} \\ H^-\left(S_i, T_i^j, n_i^j\right) &= \frac{1}{1+\left(S_i/T_i^j\right)^{n_i^j}}. \end{aligned} \tag{2}$$

When the regulator species $S_i$ approaches a threshold $T_i^j > 0$, it regulates species $S_j$. The Hill exponent $n_i^j > 0$ influences the rapidity of the regulatory process. A menstrual cycle includes both fast and slow processes. This is reflected by different exponents in the Hill functions, that is by a different steepness of the sigmoidal response curves. If the Hill exponent is high enough, the qualitative response changes rapidly within a small range of values in the independent variable, whereas for low Hill exponents ($n < 2$) the Hill function effectively behaves closer to a Michaelis–Menten type response.

Parameters and their units are given in the list of parameters in Appendix A.1. Hill thresholds and other parameters were explored

with the ABC method (Section 3), whereas the Hill exponents were adopted from previous models. Units for hormone concentrations are adopted from clinical data to enable the comparison between experimental data and simulation results. The time scale of reaction rates is 'per day'. Characteristics of the simulation results such as cycle length are on a time scale of four weeks. The model is initiated in the early follicular phase of the menstrual cycle. This phase is characterized by low concentrations of all four hormones. The initial conditions are chosen accordingly (available from the code in the GitHub repository).

Our model of the menstrual cycle can be divided into two parts. The first part describes the hormone dynamics in the hypothalamus and the pituitary. These equations are mainly based on the work of Röblitz et al. (2013) and partially overlap with other previously published models (Clark et al., 2003; Reinecke and Deuflhard, 2007; Lange et al., 2019). The second part covers follicular growth (Lange et al., 2019) and ovarian hormone dynamics. Both parts are connected through feedback interactions, which closes the loop.

### 2.1. Hypothalamus and pituitary model

GnRH is released from the hypothalamus in a pulse pattern (Carmel et al., 1976; Knobil et al., 1980; Martin et al., 1998). To account for pulsatile release, a release frequency, $freq(t)$, and amount of released GnRH, $mass(t)$, are included in the equation for the GnRH concentration, $G(t)$:

$$freq(t) = f_0 \cdot H^-\left(P4(t), T_{P4}^{freq}, n_{P4}^{freq}\right) \cdot \left(1 + H^+\left(E2(t), T_{E2}^{freq}, n_{E2}^{freq}\right)\right) \tag{3}$$

$$mass(t) = m_0 \cdot \left(H^+\left(E2(t), T_{E2}^{mass,1}, n_{E2}^{mass,1}\right) + H^-\left(E2(t), T_{E2}^{mass,2}, n_{E2}^{mass,2}\right)\right) \tag{4}$$

$$\frac{d}{dt}G(t) = mass(t) \cdot freq(t) - k_{on}^{G} \cdot G(t) \cdot R_{G,a}(t) + k_{off}^{G} \cdot GR_a(t) - k_{degr}^{G} \cdot G(t). \tag{5}$$

Hereby, $f_0$ is the basal frequency and $m_0$ the basal mass. Both are modulated by Hill functions due to the feedback actions of steroids. While P4 only has an inhibitory effect on GnRH dynamics, E2 can exhibit both positive and negative feedback actions (Nakai et al., 1978). During the luteal phase, E2 and P4 cooperatively inhibit the GnRH frequency (Goodman et al., 1981). During the period leading up to the preovulatory LH surge, E2 suppresses GnRH pulse size and thereby reduces the amount of released GnRH (Evans et al., 1994). Estradiol's feedback action on the GnRH release switches prior to ovulation from negative to positive, and thereby induces a GnRH surge in the late follicular phase (Christian and Moenter, 2010).

GnRH signalling in the pituitary is receptor mediated. The GnRH receptor belongs to the class of G-protein coupled receptors (GPCR). It is important to include the receptor binding mechanism in the model to enable simulation of drug administration. The works by Shankaran et al. (2007) and Riccobene et al. (1999) provide the basis for the receptor binding model used here. Four different receptor states are considered: (i) active GnRH receptors, $R_{G,a}$, with the ability for GnRH binding, (ii) inactive GnRH receptors, $R_{G,i}$, which are not able to bind GnRH, (iii) active GnRH-receptor complexes, $GR_a$, which mediate downstream feedback actions, and (iv) inactive GnRH-receptor complexes, $GR_i$. Table 1 lists all processes. The corresponding set of ODEs reads:

**Table 1**
Summary of all GnRH receptor binding mechanisms that are included in the model equations.

| Process | Rate |
|---|---|
| Binding of GnRH to active GnRH receptors | $k_{on}^{G} \cdot G(t) \cdot R_{G,a}(t)$ |
| Dissociation of active receptor complex | $k_{off}^{G} \cdot GR_a(t)$ |
| Recycling of inactive to active receptors | $k_{recy}^{R_{G,i}} \cdot R_{G,i}(t)$ |
| Deactivation of active to inactive receptors | $k_{inter}^{R_{G,a}} \cdot R_{G,a}(t)$ |
| Synthesis of inactive receptors | $k_{syn}^{R_{G,i}}$ |
| Degradation of inactive receptors | $k_{degr}^{R_{G,i}} \cdot R_{G,i}(t)$ |
| Inactivation of active receptor complex | $k_{inact}^{GR_a} \cdot GR_a(t)$ |
| Activation of inactive receptor complex | $k_{act}^{GR_i} \cdot GR_i(t)$ |
| Degradation of inactive GnRH receptor complexes | $k_{degr}^{GR_i} \cdot GR_i(t)$ |
| Dissociation of inactive receptor complex | $k_{diss}^{GR_i} \cdot GR_i(t)$ |

$$\frac{d}{dt}R_{G,a}(t) = k_{off}^{G} \cdot GR_a(t) - k_{on}^{G} \cdot G(t) \cdot R_{G,a}(t) - k_{inter}^{R_{G,a}} \cdot R_{G,a}(t) + k_{recy}^{R_{G,i}} R_{G,i} \tag{6}$$

$$\frac{d}{dt}R_{G,i}(t) = k_{diss}^{GR_i} \cdot GR_i(t) + k_{inter}^{R_{G,a}} \cdot R_{G,a}(t) - k_{recy}^{R_{G,i}} \cdot R_{G,i}(t) + k_{syn}^{R_{G,i}} - k_{degr}^{R_{G,i}} \cdot R_{G,i}(t) \tag{7}$$

$$\frac{d}{dt}GR_a(t) = k_{on}^{G} \cdot G(t) \cdot R_{G,a}(t) - k_{off}^{G} \cdot GR_a(t) - k_{inact}^{GR_a} \cdot GR_a(t) + k_{act}^{GR_i} \cdot GR_i(t) \tag{8}$$

$$\frac{d}{dt}GR_i(t) = k_{inact}^{GR_a} \cdot GR_a(t) - k_{act}^{GR_i} \cdot GR_i(t) - k_{degr}^{GR_i} \cdot GR_i(t) - k_{diss}^{GR_i} \cdot GR_i(t) \tag{9}$$

As suggested by Schlosser and Selgrade (2000), equations for LH and FSH are based on synthesis–release–clearance relationships. The basal LH-synthesis rate, $b_{syn}^{LH}$, is stimulated by E2 and the active GnRH-receptor complex and inhibited by P4. Eqs. (12) and (13) account for the release of LH from the pituitary into the blood stream and the related volume change. LH is cleared from the blood with a clearance rate constant $k_{cl}^{LH}$. LH dynamics are formulated as follows:

$$Syn_{LH}(t) = \frac{b_{syn}^{LH} + k_{E2}^{LH} \cdot H^+\left(E2(t), T_{E2}^{LH}, n_{E2}^{LH}\right)}{1 + k_{P4}^{LH} \cdot \left(\frac{P4(t)}{T_{P4}^{LH}}\right)^{n_{P4}^{LH}}} \cdot \left(1 + H^-\left(freq(t), T_{freq}^{LH}, n_{freq}^{LH}\right)\right) \tag{10}$$

$$Rel_{LH}(t) = \left(b_{rel}^{LH} + k_{GR_a}^{LH} \cdot H^+\left(GR_a(t), T_{GR_a}^{LH}, n_{GR_a}^{LH}\right)\right) \cdot LH_{Pit}(t) \tag{11}$$

$$\frac{d}{dt}LH_{Pit}(t) = Syn_{LH}(t) - Rel_{LH}(t) \tag{12}$$

$$\frac{d}{dt}LH_{Blood}(t) = \frac{1}{V_{Blood}} \cdot Rel_{LH}(t) - k_{cl}^{LH} \cdot LH_{Blood}(t). \tag{13}$$

FSH in the pituitary, $FSH_{Pit}$, has a synthesis rate constant $b_{syn}^{FSH}$, which is inhibited by P4 and high GnRH frequencies (Marshall and Griffin, 1993). The release of FSH from the pituitary, $Rel_{FSH}(t)$, is stimulated by the active GnRH receptor complex, $GR_a(t)$ and inhibited by the amount of E2 (Shaw et al., 2010). The transition between compartments with different sizes (pituitary to blood, blood to ovaries) is related to a change in concentration, which is included in the equations through different compartment volumes. In the ovaries, FSH

binds its receptor located at the follicles' surfaces with the binding rate $k_{on}^{FSH} \cdot R_{FSH}(t) \cdot FSH_{Ov}(t)$. FSH is cleared from the blood with clearance rate constant $k_{cl_{Blood}}^{FSH}$ and the ovaries with clearance rate constant $k_{cl_{Ov}}^{FSH}$. The ODEs describing the FSH concentrations in the system read:

$$Syn_{FSH}(t) = \frac{b_{syn}^{FSH}}{1 + \left(\frac{P4(t)}{T_{P4}^{FSH}}\right)^{n_{P4}^{FSH}}} \cdot H^{-}\left(freq, T_{freq}^{FSH}, n_{freq}^{FSH}\right) \tag{14}$$

$$Rel_{FSH}(t) = \left(b_{rel}^{FSH} + k_{GR_a}^{FSH} \cdot H^{+}\left(GR_a(t), T_{GR_a}^{FSH}, n_{GR_a}^{FSH}\right) \cdot H^{-}\left(E2(t), T_{E2}^{FSH}, n_{E2}^{FSH}\right)\right) \cdot FSH_{Pit}(t) \tag{15}$$

$$\frac{d}{dt} FSH_{Pit}(t) = Syn_{FSH}(t) - Rel_{FSH}(t) \tag{16}$$

$$\frac{d}{dt} FSH_{Blood}(t) = \frac{1}{V_{Blood}} \cdot Rel_{FSH}(t) - \left(k_{Blood}^{FSH} + k_{cl_{Blood}}^{FSH}\right) \cdot FSH_{Blood}(t) \tag{17}$$

$$\frac{d}{dt} FSH_{Ov}(t) = \frac{V_{Blood}}{V_{Ov}} \cdot k_{Blood}^{FSH} \cdot FSH_{Blood}(t) - \left(k_{on}^{FSH} \cdot R_{FSH}(t) - k_{cl_{Ov}}^{FSH_{ov}}\right) \cdot FSH_{Ov}(t) \tag{18}$$

The dynamics of the FSH receptor on the surface of follicles is modeled as follows: FSH binds to free receptors, $R_{FSH}$, with a binding rate constant $k_{on}^{FSH}$, forming a FSH-receptor complex *FSHR* that dissociates with rate constant $k_{dis}^{FSH}$. The inactive receptors $R_{FSH,dis}$ get reactivated with rate constant $k_{recy}^{FSH}$.

$$\frac{d}{dt} R_{FSH}(t) = k_{recy}^{FSH} \cdot R_{FSH,dis}(t) - k_{on}^{FSH} \cdot FSH_{foll}(t) \cdot R_{FSH}(t) \tag{19}$$

$$\frac{d}{dt} FSHR(t) = k_{on}^{FSH} \cdot FSH_{foll}(t) \cdot R_{FSH}(t) - k_{dis}^{FSH} \cdot FSHR(t) \tag{20}$$

$$\frac{d}{dt} R_{FSH,dis}(t) = k_{dis}^{FSH} \cdot FSHR(t) - k_{recy}^{FSH} \cdot R_{FSH,dis}(t). \tag{21}$$

### 2.2. Ovarian model

The authors in Lange et al. (2019) propose an ODE that describes the growth behaviour of a single follicle. We adjusted the equation and integrated hormone dependencies. Here, the size of each follicle $x_i$ which is recruited during the simulation time, is described as follows:

$$\frac{d}{dt} x_i = H^{+}(FSHR, T_{FSHR}(i), n_{FSHR}) \cdot (\xi - x_i) x_i \left(\gamma - \kappa\left(\sum_j x_j^{\nu} - \mu x_i^{\nu}\right)\right). \tag{22}$$

This equation includes follicle specific parameters as well as parameters which are shared among all follicles. The following five parameters are common for all follicles: (i) maximum size of each follicle, $\xi$, (ii) growth rate $\gamma$, (iii) strength of competition, $\kappa$, (iv) fractal dimension $\nu$, and (v) proportion of self-harm $\mu$. $\mu$ relates to the role of androgen in follicular maturation and atresia during the late follicular phase. The source of androgen are the follicles themselves, and the inhibitory effect of androgen on follicular maturation appears to be important to ensure mono-ovulation (Hillier and Tetsuka, 1997; Franks and Hardy, 2018). The parameter $\nu$ has been fixed to $\nu = 2$ in all simulations, meaning that the strength of competition is proportional to the follicular surface area. The positive Hill term in front of the equation contains a follicle specific threshold, $T_{FSHR}(i)$, which we refer to as FSH sensitivity threshold value. This follicle-specific threshold causes individual growth behaviour. Follicular growth is stimulated if the FSH-receptor complex concentration approaches and exceeds this threshold. This formulation is related to the biological finding that follicle growth does not occur below a certain level of FSH and that follicles respond differently to FSH (Brown, 1978). In our simulation, the threshold values are sampled from a normal distribution. Overall, whether a follicle starts growing depends on various factors, such as the current hormone levels, its FSH sensitivity threshold value, and the number and size of competing follicles.

We model the time points at which follicles are recruited as a Poisson point process with parameter $\lambda$ being equal to the expected number of follicles that start growing within a time interval of certain length. The Poisson parameter $\lambda$ is modulated by the FSH concentration because the number of recruited follicles is affected by the FSH level:

$$\lambda = \lambda_0 \cdot \left(1 + s_{FSH}^{Pois} \cdot H^{+}\left(FSH(T), T_{FSH}^{Pois}, n_{FSH}^{Pois}\right)\right)$$

The FSH window concept stresses the importance of elevated FSH levels for the selection of a dominant follicle (Baerwald et al., 2011; Fauser et al., 1997; Adams et al., 1993). The time period during which FSH is above a certain threshold effects the number of follicles reaching the dominant follicle's size (Schipper et al., 1998; Baird, 1990). This concept is incorporated in our model. Coupling $\kappa$, which is the parameter addressing the competition for dominance between follicles, to a negative Hill term causes an FSH-dependant decrease in follicular competition.

$$\kappa = \kappa_0 \cdot H^{-}\left(FSH, T_{FSH}^{\kappa}, n_{FSH}^{\kappa}\right). \tag{23}$$

Follicle growth is stimulated by FSH and inhibted by P4 (Baird et al., 1984). Therefore, two Hill functions modulate the growth rate $\gamma$:

$$\gamma = \gamma_0 \cdot H^{-}\left(P4, T_{P4}^{\gamma}, n_{P4}^{\gamma}\right) \cdot H^{+}\left(FSHR, T_{FSHR}^{\gamma}, n_{FSHR}^{\gamma}\right). \tag{24}$$

A major source of E2 are growing follicles and the dominant follicle produces the most E2 (Baird and Fraser, 1975; McNatty et al., 1976; Hiller et al., 1981), considered by the model with a size-dependant E2 production. We assume the E2 production by growing follicles to be proportional to the follicular surface term *FS*,

$$FS = \pi \cdot \sum H^{+}(x_i, T_{FS}, n_{FS}) \cdot (x_i)^2. \tag{25}$$

The positive Hill function with $T_{FS} = 15$ accounts for the fact that larger follicles have a higher contribution to the E2 production. The overall E2 production is the sum of basal production, $b_{syn}^{E2}$, the E2 production by follicles (first addend in Eq. 26), and the E2 production of the corpus luteum after the ovulation of a dominant follicle (second addend in Eq. 26):

$$E2(t) = b_{syn}^{E2} + s_{FS} \cdot FS + h_{E2} \cdot \exp\left(-w_{E2}(t - (T_{Ovu} + \tau))^2\right) \tag{26}$$

Similarly, P4 is produced by the corpus luteum:

$$P4(t) = b_{syn}^{P4} + h_{P4} \cdot \exp\left(-w_{P4}(t - (T_{Ovu} + \tau))^2\right) \tag{27}$$

The parameters for steroid production during the luteal phase, i.e., peak heights $h_{E2}, h_{P4}$, and inverse peak width $w_{P4}$, were estimated by fitting Gaussian curves to the data from 12 healthy patients (Fischer et al., 2021; Röblitz et al., 2013). The peaks' center position $(T_{Ovu} + \tau)$ is set with respect to the last time point of ovulation, $T_{ovu}$.

Overall, we were able to decrease the number of parameters from 119 (114 parameters in Röblitz et al. (2013) and 5 parameters in Lange et al. (2019)) to 82, mainly by replacing the heuristic description of the follicular growth dynamics used in Röblitz

et al. (2013) by the equation from Lange et al. (2019). A detailed parameter list can be found in Appendix A.1.

### 2.3. Model simulation

In the presented model, 13 ODEs and 2 algebraic equations describe the hormone dynamics. The number of ODEs describing follicular growth increases with simulation time because a new ODE is created for each follicle that is initialized at a given time point. Moreover, the model exhibits a stochastic behaviour because the initial times of follicles and the FSH sensitivity of follicles follow random processes. This causes variability within a simulation and between simulations.

Prior to the simulation, parameter values and initial conditions are loaded from files and the simulation time interval $[t_b, t_e]$ is set (Algorithm 1). In addition, the entries of an array with follicle-specific FSH sensitivity threshold values, $T_{FSHR}(i)$, are sampled from a normal distribution.

During the simulation, the global simulation time $[t_b, t_e]$ is divided into sequential time intervals $[t, t_n]$, whereby $t_n$ are either the time points at which new follicles emerge or the time points of ovulation. In any case, the simulation has to stop at these intermediate time points. This results in a more complex code structure, which is represented in Algorithm 1.

**Algorithm 1:** Model simulation

**Input**: begin time $t_b$, end time $t_e$, initial system state $x(t_b), y(t_b)$
**Output**: system state $x(t_e), y(t_e)$
  Initialize
  $t = t_b, x(t) = x(t_b), y(t) = y(t_b), startNewFollicle = 1$;
  **while** $t \leqslant t_e$ **do**
    **if** $startNewFollicle == 1$ **then**
      sample time $\tau$ at which the next follicle emerges;
      $t_{nextStart} = t + \tau$;
    **end if**
    **if** $t_{nextStart} < t_e$ **then**
      $t_n = t_{nextStart}$;
    **else if**
      $t_n = t_e$;
    **end if**
    $tspan = [t, t_n]$;
    $(x(t_f), y(t_f)), t \leqslant t_f \leqslant t_n \leftarrow$ DAE solver with event detection
    **if** $t_f < t_n$ **then**
    $startNewFollicle = 0$; ▷ovulation occurd in *tspan*
    **else if** $t_f == t_n$ **then**
      $startNewFollicle = 1$;
      **if** the right hand side of the ODE for a new follicle is positive **then**
        initiate a new follicle;
      **end if**
    **end if**
    update the destinies of all follicles;
  $t = t_f$;
**end while**

The starting time of a new follicle, $t_{nextStart}$, is determined from an exponential distribution with parameter $1/\lambda$, the inverse Poisson parameter. At each time point $t_{nextStart}$, a new follicle is initialized with size $y_0^{foll}$ and specific FSH sensitivity value $T_{FSHR}(i)$. Then the right hand side of the ODE, which can be interpreted as a growth rate corresponding to this new follicle, is evaluated. A negative right hand side means a decrease in size, i.e., the new follicle cannot start growing under the conditions at this specific time point and is hence rejected. In case of a positive growth rate, the new follicle is added to the list of active follicles and the ODE system is extended by one equation.

The time integration is evaluated by an event function that checks at every time step if an ovulation occurred. An ovulation is detected if the following two criteria are met:

- the largest follicle is at least 18 mm in size
- the value of LH is greater than the threshold parameter $T_{LH} = 25 \frac{mIU}{mL}$

Whenever the integration stops, either because ovulation occurred or because a new follicle is initiated, the destinies of all follicles are updated. For this purpose, the state of maturation for each follicle is evaluated based on the right hand side of the ODE system. Four possible follicular destinies are defined: (i) ovulation, (ii) growth, (iii) decreasing, and (iv) large but no ovulation because of too low LH concentrations.

The simulation output covers time courses of hormone concentrations and follicles' diameters. In addition to that, there is a readout of the number and time points of ovulation and cycle lengths. The model and the simulation algorithm have been implemented in *MATLAB* and are accessible on *GitHub* (https://github.com/SoFiwork/GynCycle_newVersion). Numerical simulations have been performed using the ODE solver *ode15s*.

## 3. Methods

We used Approximate Bayesian Computation (ABC) with summary statistics to investigate the parameter space. The goal is to find parameters that have narrow value ranges and that can therefore be interpreted as sensitive, and to find parameter clusters.

### 3.1. Population of models, model checking, and sensitivity analysis

Sensitivity analysis methods help to understand how uncertainty and noise in the model input effect the model output and its ambiguity. Classical sensitivity analysis algorithms evaluate model outputs at specific time points. However, these methods are not applicable to the presented model because of variation in simulation results, such as cycle length and composition of follicular cohorts, prevent the specification of a set of evaluation time points. Alternatively, ABC can be used to study parameter spaces and sensitivities and to estimate parameters. The overall idea of all ABC-based approaches is to bypass the evaluation of a likelihood function by performing high numbers of simulations which are compared to observed data (Toni et al., 2009). Our ABC algorithm is based on the ABC rejection sampler introduced by Pritchard et al. (1999) and consists of the following four steps:

1. A parameter vector $\hat{\theta}$ is sampled from a prior distribution $\pi(\theta)$.
2. Using $\hat{\theta}$ as model parameters, a data set $\widehat{D}$ is generated by simulation.
3. $\widehat{D}$ is evaluated with respect to a set of defined criteria and will either be accepted or rejected.
4. Return to step 1.

We defined two sets of prior distributions: (i) $\pi(\theta)_{Hormones}$ for parameters associated with hormone dynamics, and (ii) $\pi(\theta)_{Follicles}$ for parameters used in the follicular growth equation. Parameters that were used to create the two model populations are marked (*) in the parameter list given in Appendix A.1. In all cases, model parameters were sampled from uni-variate log normal prior distributions with mean $\mu = \theta_0$, where $\theta_0$ denotes the original parameter value (Appendix A.1), and standard deviation $\sigma = 0.15$.

The comparison between simulations is challenging because of the stochastic elements included in the model. The composition of follicle cohorts varies between simulations because the time points of follicle initialization and the follicle-specific sensitivities to FSH are sampled prior to each simulation run. Differences in the follicular cohort composition influence the hormone dynamics and the selection of the dominant follicle. To study the effects of variation in the model parameters on the simulation results, we needed to ensure that the effects we observe are not caused by differences in follicular cohort composition. Therefore, the initialization time points and FSH sensitivity values of the follicles were fixed for all simulations performed for the ABC analysis. However, we still observe variations in cycle length and offset between simulations with different parametrizations. Therefore, a distance function to evaluate the difference between $\hat{D}$ and $D$ is not applicable. Instead, the following three characteristics (Fig. 2) were assessed as summary statistics for each simulation run and were used for the comparison.

- At least 75% of the FSH profiles of consecutive cycles have to follow a characteristic profile as it is illustrated in Fig. 2.
- The mean cycle length has to be between 21 and 40 days (Rosenfield, 2013 and National Health Service, 2021 state that most cycles are within this range.)
- The variability in cycle length needs to be smaller than 4 days.

The simulation time was set to 300 days, which ensures that about 13 consecutive menstrual cycles can be evaluated (Fig. 2a). The FSH profile of each simulated cycle was evaluated automatically by checking three properties which give the profile its characteristic shape (Fig. 2b):

- decrease of the FSH concentration between 5 and 3 days before ovulation
- increase of the FSH concentration right before ovulation
- decrease of the FSH concentration after ovulation

Each cycle within a simulation run was marked by the ovulation of the dominant follicle. This characteristic time point was used as a reference time point to calculate the average rate of change of the FSH profile within a defined time interval. The cycle length of all menstrual cycles within one simulation was also evaluated automatically by measuring the time difference from one ovulation to the next one (Fig. 2a).

We observed that in simulations with a regular FSH profile, also the remaining hormone profiles are physiologically reasonable.We therefore only analysed FSH profiles for the summary statistics. This observation can certainly be attributed to the fact that the model represents a fully closed feedback loop.

Based on the summary statistics, simulation runs were classified as successful or unsuccessful, whereby successful simulations constitute a virtual patient population. A simulation was classified as successful if all of the above criteria were satisfied. For each parameter we thus obtained one distribution from successful simulations and one distribution from unsuccessful ones. The similarity between these two discrete distributions was evaluated using the Jensen–Shannon divergence, which is a symmetric and smoothed formulation of the Kullback–Leibler divergence (Lin, 1991).

### 3.2. Parameter clustering

For each of the two model populations, created by variation in either the follicle or the hormone parameters, the parameter spaces of the two subgroups (accepted and rejected simulations) were analysed with the aim to find parameter dependencies and clusters. By comparing the individual parameter distributions of successful and unsuccessful simulations, we explore differences in the parameter ranges between these two groups.

For this purpose, we applied a spectral clustering method, the robust Perron cluster analysis (PCCA+) (Röblitz and Weber, 2013), to a pairwise similarity matrix. The similarity between two parameter vectors $i$ and $j$, $s_{ij}$, was derived from the pairwise distance $d_{ij}$ as $s_{ij} = 1 - d_{ij}$, whereby pairwise distances were normalized such that $\max_{i,j} d_{i,j} = 1$. For the distance measure $d_{ij}$, we used a path-based distance measure based on connectedness rather than compactness (Fischer et al., 2001). This criterion captures data sources that are spread out on a low-dimensional manifold which is embedded in a high dimensional data space. The connectedness criterion considers two objects as similar if there exists a mediating path without an edge with large cost, whereby we used the Euclidian distance as cost function. This distance can be computed by solving the minimax path problem (also called bottleneck shortest path problem) on the complete undirected graph, which asks for the path between two points that minimizes the maximum edge capacity. We used the minimax variant of the Floyd-Warshall algorithm to solve this problem.

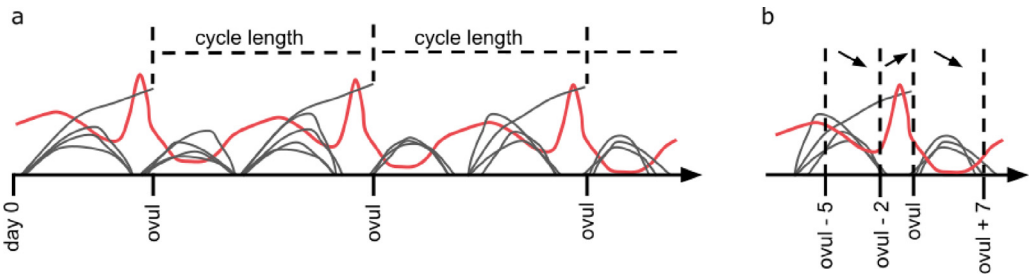


**Fig. 2.** Sketch of simulation results to illustrate the assessment of summary statistics. Grey lines are individual ovarian follicles. The FSH profile is given in red. Ovulations (ovul) of a dominant follicle are marked by terminating growth trajectories. a) Within each simulation multiple consecutive menstrual cycles are observed. A cycle is defined from one ovulation of a follicle to the next one. b) The shape of each FSH profile is evaluated based on three characteristic slopes: i) a decrease during the late follicular phase (five to two days prior to ovulation), (ii) an increase during the two days before ovulation, and (iii) a decrease during the luteal phase (during seven days after ovulation).

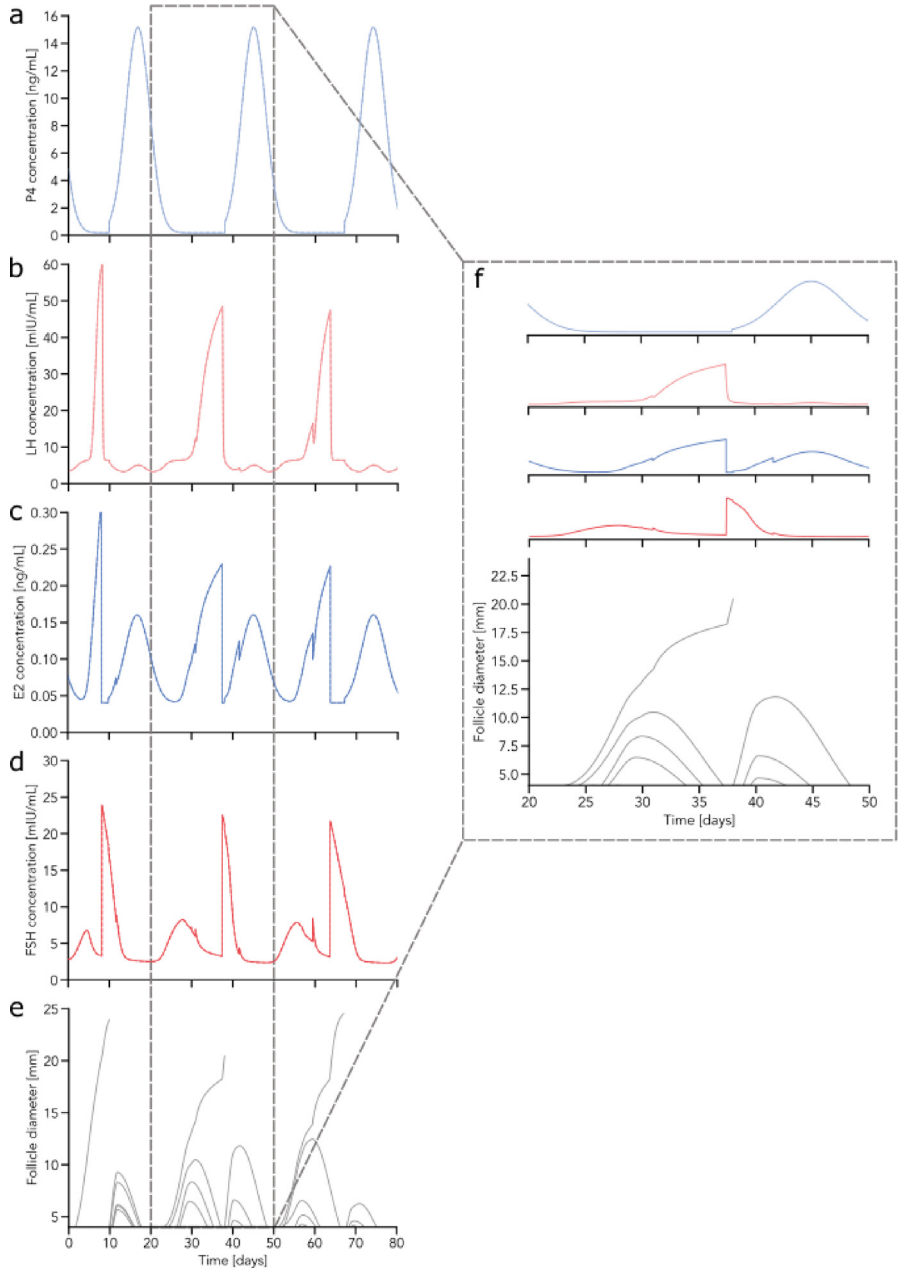


**Fig. 3.** Example simulation of three consecutive cycles. Panels a-d) show the time-evolution of the four hormones P4, LH, E2, and FSH. Panel e) illustrates the growth trajectories of follicles within this time frame. Panel f) is a zoom into the second cycle represented on the left.

## 4. Results

### *4.1. Model simulation*

The model enables simulations of consecutive cycles as represented in Fig. 3, which displays simulated follicular growth trajectories (Fig. 3e) and hormone profiles (Fig. 3a-d) of three menstrual cycles originating from the same simulation. The zoom in panel (3f) showcases the interplay between follicular growth and hormone dynamics. Fundamental features of the interaction are apparent. Follicles grow under elevated FSH levels and the peak in LH concentration triggers the ovulation of the largest active follicle. Increased P4 concentrations during the luteal phase prevent the growth of any large follicles.

Furthermore, follicles grow in cohorts/waves consisting of about five follicles. The property that follicles grow in distinct cohorts (one cohort during the follicular phase and one during the luteal phase) is not implemented in the model itself. This emergent behaviour is rather a result of the interplay between hormones and follicles covered by the model. The elevated P4 levels during the luteal phase prevent ovulation. Hence, there is no dominant follicle when the P4 level is high. The ovulation of the dominant follicle, which is visible as a terminated growth trajectory around day 15, is aligned with the LH peak.

Fig. 4 shows the hormone profiles (LH, FSH, E2, and P4) of three consecutive cycles and pooled hormone data for one menstrual cycle from 12 healthy women (data set from Röblitz et al., 2013). The three consecutive cycles originating from one simulation and were overlaid by shifting them along the time axis. All curves are aligned on the day of ovulation. Simulated peak concentrations and concentration ranges agree with the data set. The overall shape of simulated hormone profiles are also comparable to the data. The

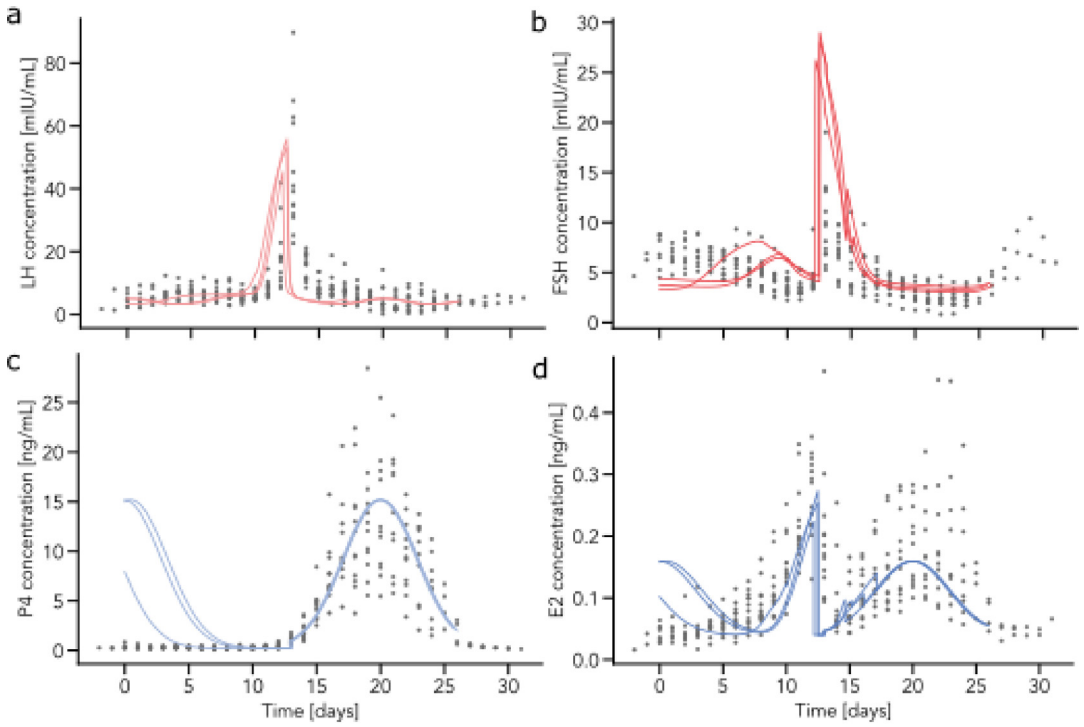


**Fig. 4.** Comparison of simulated hormone profiles for LH, FSH, P4 and E2 and pooled hormone data from 12 healthy women. Simulated hormone profiles and measurement data are aligned with the ovulation at day 13. Grey dots represent the pooled data set. For each hormone, three consecutive cycles are overlaid.

simulated cycle lengths range from 22.7 to 27.8 days. A detailed overview of the cycle length distribution is presented in Appendix A.2.

However, there are notable discrepancies between the data and the simulation results. The measured FSH profiles show a longer rise of FSH during the follicular phase from day 1 to day 10 (Fig. 4b). The simulated LH peak is shifted to the left compared to the peak in the data (Fig. 4 a). There is also a mismatch between the data and the simulated hormone profile for E2 during the early follicular phase up to day 5 (Fig. 4a).

### 4.2. Model Analysis

To investigate the parameter space, we created two populations of models, one focusing on hormone dynamics and one focusing on follicular growth behaviour. Each population is composed of 1000 parameter realizations. Follicles were initialized with the same follicle-specific properties (FSH sensitivity and start times) to ensure that variability is not caused by changes in the initial composition of the cohort of follicles. Each simulation was checked automatically according to the shape of the FSH profile, the cycle length and its variability (Fig. 2). A simulation that meets all three criteria was categorized as successful. Since the duration of a cycle is measured from one ovulation to the next one, ovulations of two follicles shorty after each other cause an incorrect cycle length. Hence, successful simulations contain only mono-ovulatory cycles. This bias is negligible, because we rarely observed the ovulation of multiple follicles around mid-cycle in our simulation results.

Figs. 5a) and b) show the numbers of successful and unsuccessful simulations in the two populations of models. For both populations about 1/3 of the parameter realizations give successful simulations. The event plots in Figs. 5c) and d) illustrate the criteria on which 100 randomly selected unsuccessful simulations failed. In all of these 100 simulations, it is the FSH profile that does not satisfy the criteria, whereas in both model populations abnormal cycle length or cycle length variability are less often the reason for failure.

Fig. 5e) shows the distribution for the model parameter $\mu$, which is one of the parameters varied to create the follicle specific model population. The distribution of $\mu$ differs between successful simulations (green histogram) and unsuccessful simulations (red histogram), with a Jensen-Shannon divergence of 0.13. For all other parameters striking differences are not present (Figs. A.7 and A.8). Using Pearson correlation, we investigated the relationship between $\mu$ and the average cycle length as well as between $\mu$ and the variance of the cycle length. A negative linear correlation was found between $\mu$ and the average cycle length (Pearson correlation coefficient = $-0.71$, see Fig. 5f). The analysis was repeated for an alternative follicle initialization, which gave comparable results (A.4).

By applying a clustering method on the multivariate parameter distributions, we aimed at finding parameter clusters to classify simulations. Our hypothesis was that parameters that lead to successful and unsuccessful simulations, respectively, will fall into different clusters. We applied PCCA+, which did not indicate any clusters in the parameter space.

## 5. Discussion

This work presents and explores a novel mathematical model of the menstrual cycle, which combines hormone dynamics and follicular growth in a mechanistic manner. None of the previously published models allowed for simultaneously simulating hormone dynamics and follicular maturation throughout consecutive menstrual cycles. The applicability of our model in a medical setting is demonstrated in Fischer et al. (2021), which can be considered as a validation for the presented model.

The growth of ovarian follicles in cohorts of about five follicles can be observed as an emerging property in our simulation results. While the growth of ovarian follicles in cohorts is a well-described

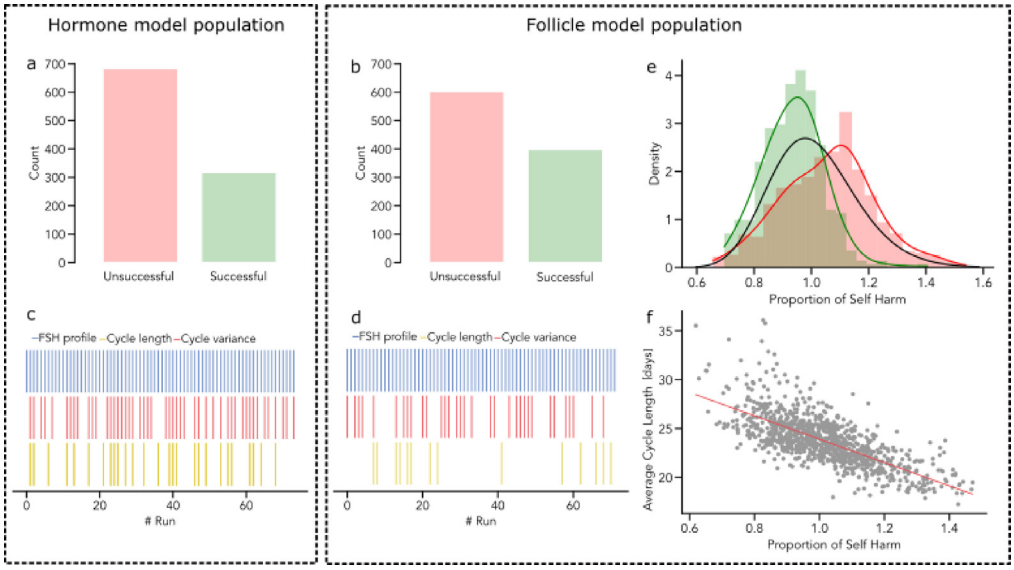


**Fig. 5.** Summary of the model analysis. The left box sums up results for the population of models that resulted from variation of parameters important for hormone dynamics, whereas the right box shows results for the model population based on variation of follicle parameters. Each population consists of 1000 randomly drawn parameter realizations. Histograms in Figures a) and b) present the count of successful (green) and unsuccessful (red) simulations for each population of models. The event plots in Figures c) and d) illustrate the cause of failure for 100 failed simulations from each population (top/blue: failure due to irregular FSH profile, middle/red: failure due to abnormal cycle length, bottom/yellow: failure due to abnormal cycle length variability). Figure e) shows the distribution of parameter $\mu$, which is the proportion of self harm included in the follicle growth equation. The solid black line shows the prior distribution of $\mu$ used for sampling. The green and red distributions are the parameter distributions for successful and unsuccessful simulations, respectively (Jensen-Shannon divergence = 0.13). Figure f) demonstrates the negative linear correlation between $\mu$ and the average cycle length (Pearson correlation coefficient = −0.71).

phenomenon in some mono-ovulatory species such as cattle, it counts as hypothesis in human. Our model can be considered as further evidence that follicular waves also occur in human.

Differeences between patients' data and simulation trajectories are visible in Fig. 4. We argue that the difference in cycle length contributes to the mismatches. The simulated average cycle length ranges from 22.7 to 27.8 days (Fig. A.6), which is within the physiological range (Bull et al., 2019). The cycle length is unfortunately not specified in the data set, but we estimated it to be about 28 days. Therefore, simulated cycles can be about five days shorter than in the data set. In line with the literature (Bull et al., 2019), we implemented the model in a way that little variation occurs in the length of the luteal phase. It is therefore the follicular phase that causes variation in cycle length and that is responsible for shorter simulated cycles (compared to the duration of the follicular phase in the patients' data). A shorter follicular phase in the simulations compared to the data explains the shift of the LH peak as well as the shorter period of the FSH rise.

It is also important to note that neither the parameters in the follicle model nor in the equations for E2 and P4 were optimized using these data, in contrast to the parameters in the hormone model, which had previously been estimated from these data (Röblitz et al., 2013). Therefore, a re-parameterization of the model could improve the difference between data and simulation curves, but parameter estimation for the given model is challenging. Most of the parameters included in the current model version are non-identifiable given the available data. One reason is that there is simply not enough data available given the complexity of the model.

The balance between available data and model parameters could be improved with a systematic model reduction. However, this would result in losing parts of the model for which no measurement data are available at the moment, e.g., the GnRH receptor binding model. By removing that part of the model, treatments with GnRH analogues could not be simulated any more.

Moreover, the data we could access only covers hormone profiles for one cycle, and does not provide any information about individuals' cycle lengths or variability. Since our model simulates consecutive cycles, data sets covering multiple menstrual cycles would be preferable.

We used an ABC-based approach to investigate model parameters in more depth. Our hypothesis was that parameters for successful/unsuccessful simulations would form clusters. However, PCCA + cluster analysis did not reveal clusters in the parameter space. We conclude that there is no particular subset of parameters that leads to non-biological simulation results. Instead, our analysis indicates that the composition of the complete parameter set determines the fate of a simulation.

By comparing the parameter distributions or each parameter with respect to the simulation fate of successful and unsuccessful simulations, we did not find parameters that are restricted to narrow ranges of values. This leads us to the conclusion that non of the selected parameters is particularly sensitive. A clear limitation of our approach is that the parameter distributions were not derived from data.

Based on the Jensen–Shannon divergence, the distribution of $\mu$ differs between successful and unsuccessful simulations. The correlation between $\mu$ and the cycle length is in line with biological knowledge. $\mu$ encodes a process that results in follicle atresia. Hence, if $\mu$ is higher, more follicles undergo atresia, which reduces competition and results in earlier emergence of a dominant follicle.

As demonstrated in Fischer et al. (2021), the model can be used to simulate controlled ovarian stimulation protocols. However, the model formulation does not allow for an application to all pathological cases. The mathematical formulation of the follicular growth adopted from Lange et al. (2019) does not allow for the arrest of multiple premature follicles as it is described for the Polycystic Ovary Syndrome (PCOS). Therefore, this model is not eligible to describe PCOS or to simulate ovarian stimulation protocols in PCOS patients. Cell-based models of follicular morphogenesis such as the one proposed in Monniaux et al. (2016) could allow for a simulation-based exploration of PCOS. Note that the model could potentially also be used to further investigate the relationship between follicles in mono-ovulatory species compared to poly-

ovulatory species, since these mechanisms are still poorly understood (Sirotkin et al., 2017).

To conclude, our presented modelling approach is the first one that allows for simulation-based studies of the interplay between hormones and ovarian follicles throughout consecutive menstrual cycles. Therefore, it can be used to test new treatment strategies for ovarian hyper stimulation in silico. Our simulation results display variability in the cycle dynamics as a result of stochasticity in the recruitment process of follicles. To our knowledge, none of the previously published models contains stochastic elements resulting in variability between cycles, which resembles intra-individual variability. The growth of follicles in cohorts is an emergent property of the implemented mechanistic interactions between hormones and follicles, which supports the follicular wave theory in humans. Re-parameterization of the model could increase its predictive values, but this would require longitudinal ultrasound measurements of follicles as well as hormone profiles throughout consecutive cycles from several individuals.

## CRediT authorship contribution statement

**Sophie Fischer-Holzhausen:** Methodology, Validation, Visualization, Writing - original draft, Writing - review & editing. **Susanna Röblitz:** Conceptualization, Supervision, Methodology, Writing - original draft, Writing - review & editing.

## Declaration of Competing Interest

The authors declare that they have no known competing financial interests or personal relationships that could have appeared to influence the work reported in this paper.

## Acknowledgments

The work of SF and SR was supported by the Trond Mohn Foundation (BSF, https://www.mohnfoundation.no/), Grant No. BFS2017TMT01. The funder had no role in study design, data collection and analysis, decision to publish, or preparation of the manuscript.

## Appendix A. Supplementary data

Supplementary data associated with this article can be found, in the online version, at https://doi.org/10.1016/j.jtbi.2022.111150.

## References

Adams, G., Kot, K., Smith, C., Ginther, O., 1993. Selection of a dominant follicle and suppression of follicular growth in heifers. Animal Reproduction Science 30 (4), 259–271.
Baerwald, A., Adams, G., Pierson, R., 2011. Ovarian antral folliculogenesis during the human menstrual cycle: A review. Human Reproduction Update 18 (1), 73–91.
Baird, D., 1990. The selection of the follicle of the month, in: From Ovulation to Implantation Proceedings of the VII Regnier de Graaf Symposium. Maastricht, the Netherlands: Excerpta Medica, 384, 1990..
Baird, D., Fraser, I., 1975. Concentration of oestrone and oestradiol in follicular fluid and ovarian venous blood of women. Clin. Endocrinol. 4 (3), 259–266.
Baird, D.T., Bäckström, T., McNeilly, A.S., Smith, S.K., Wathen, C.G., 1984. Effect of enucleation of the corpus luteum at different stages of the luteal phase of the human menstrual cycle on subsequent follicular development. J. Reprod. Fertil. 70 (2), 615–624.
Bakos, O., Lundkvist, Ö., Wide, L., Bergh, T., 1994. Ultrasonographical and hormonal description of the normal ovulatory menstrual cycle. Acta obstetricia et gynecologica Scandinavica 73 (10), 790–796.
Brown, J., 1978. Pituitary control of ovarian function–concepts derived from gonadotrophin therapy. Aust. N. Z. J. Obstet. Gynaecol. 18 (1), 47–54.
Bull, J.R., Rowland, S.P., Scherwitzl, E.B., Scherwitzl, R., Danielsson, K.G., Harper, J., 2019. Real-world menstrual cycle characteristics of more than 600,000 menstrual cycles. NPJ Digital Med. 2 (1), 1–8.
Carmel, P., Araki, S., Ferin, M., 1976. Pituitary stalk portal blood collection in rhesus monkeys: evidence for pulsatile release of gonadotropin-releasing hormone (GnRH). Endocrinology 99 (1), 243–248.
Chavez-Ross, A., Franks, S., Mason, H., Hardy, K., Stark, J., 1997. Modelling the control of ovulation and polycystic ovary syndrome. J. Math. Biol. 36 (1), 95–118.
Christian, C.A., Moenter, S.M., 2010. The neurobiology of preovulatory and estradiol-induced gonadotropin-releasing hormone surges. Endocrine Rev. 31 (4), 544–577.
Clark, L.H., Schlosser, P.M., Selgrade, J.F., 2003. Multiple stable periodic solutions in a model for hormonal control of the menstrual cycle. Bull. Math. Biol. 65 (1), 157–173.
Clément, F., Gruet, M., Monget, P., Terqui, M., Jolivet, E., Monniaux, D., 1997. Growth kinetics of the granulosa cell population in ovarian follicles: an approach by mathematical modelling. Cell proliferation 30 (6–7), 255–270.
Evans, N., Dahl, G., Glover, B., Karsch, F., 1994. Central regulation of pulsatile gonadotropin-releasing hormone (GnRH) secretion by estradiol during the period leading up to the preovulatory GnRH surge in the ewe. Endocrinology 134 (4), 1806–1811.
Fauser, B.B., van Heusden, A.M., 1997. Manipulation of human ovarian function: physiological concepts and clinical consequences, Endocrine Reviews..
Fischer, B., Zoller, T., Buhmann, J.M., 2001. Path Based Pairwise Data Clustering with Application to Texture Segmentation, in: International Workshop on Energy Minimization Methods in Computer Vision and Pattern Recognition (EMMCVPR) 2001, Lecture Notes in Computer Science, Springer-Verlag, Berlin Heidelberg, 235–250..
Fischer, S., Ehrig, R., Schäfer, S., Tronci, E., Mancini, T., Egli, M., Ille, F., Krüger, T.H., Leeners, B., Röblitz, S., 2021. Mathematical Modeling and Simulation Provides Evidence for New Strategies of Ovarian Stimulation. Front. Endocrinol. 12, 117.
Fortune, J., 1994. Ovarian follicular growth and development in mammals. Biol. Reproduction 50 (2), 225–232.
Franks, S., Hardy, K., 2018. Androgen action in the ovary. Front. Endocrinol. 9, 452.
Speroff, L., Fritz, M.A., 2005. Clinical gynecologic endocrinology and infertility. Lippincott Williams & wilkins.
Goodman, R.L., Bittman, E.L., Foster, D.L., Karsch, F.J., 1981. The endocrine basis of the synergistic suppression of luteinizing hormone by estradiol and progesterone. Endocrinology 109 (5), 1414–1417.
Harlow, S.D., 2000. 9 – Menstruation and Menstrual Disorders: The Epidemiology of Menstruation and Menstrual Dysfunction, in: M.B. Goldman, M.C. Hatch (Eds.), Women and Health, Academic Press, San Diego, 99–113, ISBN 978-0-12-288145-9, 2000..
Hiller, S.G., Reichert, L.E., Van Hall, E.V., 1981. Control of preovulatory follicular estrogen biosynthesis in the human ovary. J. Clinical Endocrinol. Metabolism 52 (5), 847–856.
Hillier, S.G., Tetsuka, M., 1997. 3 Role of androgens in follicle maturation and atresia. Bailliere's Clinical Obstetrics Gynaecology 11 (2), 249–260.
Knobil, E., Plant, T., Wildt, L., Belchetz, P., Marshall, G., 1980. Control of the rhesus monkey menstrual cycle: permissive role of hypothalamic gonadotropin-releasing hormone. Science 207 (4437), 1371–1373.
Lacker, H.M., Akin, E., 1988. How do the ovaries count? Math. Biosci. 90 (1–2), 305–332.
Lange, A., Schwieger, R., Plöntzke, J., Schäfer, S., Röblitz, S., 2019. Follicular competition in cows: the selection of dominant follicles as a synergistic effect. J. Math. Biol. 78 (3), 579–606.
Lin, J., 1991. Divergence measures based on the Shannon entropy. IEEE Trans. Inform. Theory 37 (1), 145–151.
Marshall, J., Griffin, M., 1993. The role of changing pulse frequency in the regulation of ovulation. Human Reproduction 8 (suppl_2), 57–61.
Martin, K.A., Welt, C.K., Taylor, A.E., Smith, J.A., Crowley Jr, W.F., Hall, J.E., 1998. Is GnRH Reduced at the Midcycle Surge in the Human? Neuroendocrinology 67 (6), 363–369.
McNatty, K., Baird, D., Bolton, A., Chambers, P., Corker, C., McLean, H., 1976. Concentration of oestrogens and androgens in human ovarian venous plasma and follicular fluid throughout the menstrual cycle. J. Endocrinol. 71 (1), 77–85.
Monniaux, D., Michel, P., Postel, M., Clément, F., 2016. Multi-scale modelling of ovarian follicular development: From follicular morphogenesis to selection for ovulation. Biol. Cell 108 (6), 149–160.
Nakai, Y., Plant, T., Hess, D., Keogh, E., Knobil, E., 1978. On the sites of the negative and positive feedback actions of estradiol in the control of gonadotropin secretion in the rhesus monkey. Endocrinology 102 (4), 1008–1014.
National Health Service (NHS), Periods and fertility in the menstrual cycle, https://www.nhs.uk/conditions/periods/fertility-in-the-menstrual-cycle/, 2021..
Pritchard, J.K., Seielstad, M.T., Perez-Lezaun, A., Feldman, M.W., 1999. Population growth of human Y chromosomes: a study of Y chromosome microsatellites. Mol. Biology Evol. 16 (12), 1791–1798.
Reinecke, I., Deuflhard, P., 2007. A complex mathematical model of the human menstrual cycle. J. Theor. Biol. 247 (2), 303–330.
Riccobene, T.A., Omann, G.M., Linderman, J.J., 1999. Modeling activation and desensitization of G-protein coupled receptors provides insight into ligand efficacy. J. Theor. Biol. 200 (2), 207–222.
Röblitz, S., Weber, M., 2013. Fuzzy spectral clustering by PCCA+: application to Markov state models and data classification. Adv. Data Anal. Classif. 7 (2), 147–179.
Röblitz, S., Stötzel, C., Deuflhard, P., Jones, H.M., Azulay, D.-O., van der Graaf, P.H., Martin, S.W., 2013. A mathematical model of the human menstrual cycle for the administration of GnRH analogues. J. Theor. Biol. 321, 8–27.

Rosenfield, R.L., 2013. Adolescent anovulation: maturational mechanisms and implications. J. Clinical Endocrinol. Metabolism 98 (9), 3572–3583.
Schipper, I., Hop, W.C., Fauser, B.C., 1998. The follicle-stimulating hormone (FSH) threshold/window concept examined by different interventions with exogenous FSH during the follicular phase of the normal menstrual cycle: duration, rather than magnitude, of FSH increase affects follicle development. J. Clinical Endocrinol. Metabolism 83 (4), 1292–1298.
Schlosser, P.M., Selgrade, J.F., 2000. A model of gonadotropin regulation during the menstrual cycle in women: Qualitative features. Environ. Health Perspectives, 873–881.
Selgrade, J.F., 2001. Modeling hormonal control of the menstrual cycle. Comments Theor. Biol. 6 (1), 79–101.
Shankaran, H., Wiley, H.S., Resat, H., 2007. Receptor downregulation and desensitization enhance the information processing ability of signalling receptors. BMC Systems Biol. 1 (1), 1–15.
Shaw, N., Histed, S., Srouji, S., Yang, J., Lee, H., Hall, J., 2010. Estrogen negative feedback on gonadotropin secretion: evidence for a direct pituitary effect in women. J. Clinical Endocrinology Metabolism 95 (4), 1955–1961.
Sinisi, S., Alimguzhin, V., Mancini, T., Tronci, E., Mari, F., Leeners, B., 2020. Optimal personalised treatment computation through in silico clinical trials on patient digital twins. Fundamenta Informaticae 174 (3–4), 283–310.
Sinisi, S., Alimguzhin, V., Mancini, T., Tronci, E., Leeners, B., 2020. Complete populations of virtual patients for in silico clinical trials, Bioinformatics..
Sirotkin, A.V., Florkovičová, I., Schaeffer, H.-J., Laurincik, J., Harrath, A.H., 2017. Interrelationships between ovarian follicles grown in culture and possible mediators. Reprod. Biol. 17 (1), 97–104.
Toni, T., Welch, D., Strelkowa, N., Ipsen, A., Stumpf, M.P., 2009. Approximate Bayesian computation scheme for parameter inference and model selection in dynamical systems. J. R. Soc. Interface 6 (31), 187–202.